ELSEVIER

Solid State Ionics 131 (2000) 23–33

SOLID STATE IONICS

www.elsevier.com/locate/ssi

Structure formation in diffusional growth and dewetting

E. Brener[1], H. Müller-Krumbhaar*, D. Temkin, T. Abel

Institut für Festkörperforschung, Forschungszentrum Jülich, D-52425 Jülich, Germany

Received 30 April 1998; accepted 31 August 1998

Abstract

The morphology diagram of possible structures in two-dimensional diffusional growth is given in the parameter space of undercooling Δ versus anisotropy of surface tension ϵ. The building block of the dendritic structure is a dendrite with a parabolic tip, and the basic element of the seaweed structure is a doublon. The transition between these structures shows a jump in the growth velocity. We show the analogy of diffusional growth with dewetting patterns of a fluid film on a substrate. We also describe the structures and velocities of fractal dendrites and doublons destroyed by noise. The extension of these results to three-dimensional growth is briefly discussed.

1. Introduction

During the last few years, our understanding of pattern formation in various non-linear dissipative systems has made remarkable progress. Building on these foundations, it has now become possible to develop a description of a large class of patterns that are found in diffusional growth. This leads to the construction of a *morphology diagram* and to predictions concerning the *transitions* between the different structures [1,2].

To introduce the topic, let us take a look at a few interesting patterns appearing in nature and experiments. Fig. 1 displays one of the most popular examples which has become a paradigm of the field: the snowflake. It also happens to be the first case of

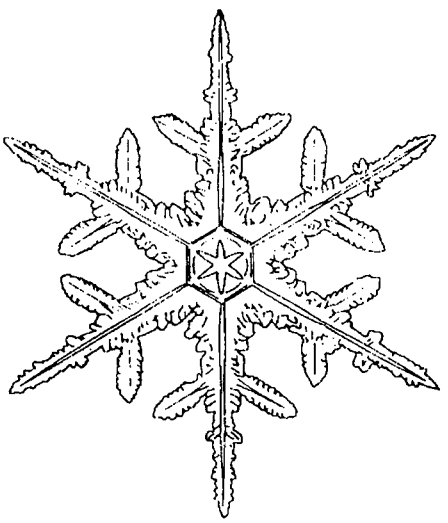

Fig. 1. Drawing of a snowflake, adapted from a photograph by Kobayashi and Kuroda [3].

*Corresponding author. Tel.: +49-2461-613-428; fax: +49-2461-612-620.

E-mail address: h.mueller-krumbhaar@fz-juelich.de (H. Müller-Krumbhaar)

[1]On leave from ISSP RAN, Chernogolovka, 142432, Russia.

0167-2738/00/$ – see front matter
PII: S0167-2738(00)00619-6

spontaneous pattern formation in nature that has been treated scientifically (rather than as a theological topic) in a publication. In his article on 'The Six-Cornered Snowflake' [4], Kepler speculated that the six-fold symmetry of snowflakes has to do with something we would call the crystal structure today. He also arrived at the conclusion that a detailed understanding of snowflakes was beyond his reach. Just how judicious this modest statement was, may be gathered from the fact that even 10 years ago, more than 350 years after Kepler, the basic mechanism by which the characteristic length scales of snowflake patterns arise was not known.

Snowflakes are ice crystals growing from a critical nucleus in an environment of supercooled vapor. The condensation process clearly is a first-order phase transition. Contrary to second-order transitions, first-order ones give rise to a sharp interface between the two phases. It is the dynamics of this interface that are of interest here.

Snowflakes are flat objects of approximate but not exact hexagonal symmetry. Their six main arms have a characteristic structure: they emit sidebranches at crystallographic angles. When these structures were given names, classical education was still prevailing, so they were called dendrites, after the greek '*τό δένδρον*', meaning 'the tree'.

No two snowflakes are alike. Therefore, their shape must be extremely sensitive to the environmental changes brought about by their turbulent motion within the cloud. On the other hand, the six arms are very similar to each other. Hence, on the length scale of the size of a snowflake (1 cm), its environment must be spatially *homogeneous*.

The question then arises why such a *complex morphology* evolves in a uniform environment — why not simply spheres? Or, if the crystalline anisotropy plays a role, why not just hexagonal plates (according to the crystal system of ice)?

Another question that we may naturally ask is: how does the snowflake *select* its typical length scales, e.g. the tip radius of its main arms, the width and spacing of the sidebranches?

The growth dynamics of true snowflakes are complicated by several circumstances — there is a large density difference between the solid and the vapor; besides the vapor there is a second agent for heat transport, namely air; furthermore, the temporal fluctuations of the environment of a flake are strong.

Clearly, it will be much easier to understand the essential mechanisms by analysing experiments which are simple to prepare and still produce dendrites. Some most careful and beautiful experiments of this kind have been done in the group of Glicksman [5–8]. They consist of chemically pure succinonitrile [$C_2H_4(CN)_2$], which is an important model substance because, being transparent, it can be easily observed during solidification, while its solidification properties are similar to those of (technologically important) metals. The solid phase grows into an undercooled melt. There are no facets on the crystal, its surface is rough. This means that the attachment kinetics of molecules at the interface are very fast — the free energy for the formation of a step on the interface is zero, there is no nucleation barrier. Thus kinetics are not a limiting factor in the growth process. Growth is controlled by how fast latent heat produced in the solidification process can be transported away via diffusion. (In the case of the snowflake, this is not true for the third dimension; growth in that direction is faceted, keeping the flake essentially two-dimensional.)

The main result of these experiments to be kept in mind is that, given the undercooling, the dendrite has both a *uniquely selected tip radius and constant velocity*.

Completely different structures are commonly formed by minerals crystallizing from viscous magmas or by certain polymers solidifying from the melt [9], so-called spherulites. Contrary to dendrites, spherulites are polycrystalline. They have approximately radial symmetry and their substructures are not oriented along crystallographic directions.

Their radius grows proportional with time, which means they have a stationary growth phase. Again, one would like to be able to make predictions about selected length scales.

It was proposed by Goldenfeld [9] that spherulites are three-dimensional examples for a growth structure which was then called 'dense branching morphology' and will be described shortly. Experimentally, densely branching patterns were first obtained in a non-crystalline system; this was the viscous fingering experiment in a circular Hele–Shaw cell [10]. An inviscid fluid is injected into a viscous one, displacing it and forming branchy structures in the process. It is still controversial [11,12] whether in such a system, governed by the Laplace instead of

the diffusion equation, the dense branching morphology can persist at large length scales.

There are well-known growth models, most notably diffusion-limited aggregation (DLA), that lead to the formation of *fractal* patterns [13].

Since DLA is a Laplacian system, it is natural to ask whether fractal structures are to be expected in diffusional growth, too.

An obvious classification of growth structures would then be to distinguish between *compact* and *fractal* patterns [1,2]. By compact growth we mean growth at a constant (average) density, irrespective of the value of this density. As we shall see later, fractal patterns in crystal growth are fractal only up to a certain size and compact beyond.

What we are aiming at is to formulate a theory that relates the diverse discussed patterns in some kind of *kinetic phase diagram*. The 'kinetic' used here reminds us that we are not dealing with phase transitions (which would imply thermodynamic equilibrium), but dynamic states manifesting themselves in typical growth patterns. In the literature, the term *morphology diagram* is widely used [14].

On the one hand, such a diagram indicates which patterns are selected for which system parameters. Its existence signifies, in particular, that there is a certain degree of independence of the observed morphologies of initial conditions. On the other hand, given the existence of such a diagram, one may try to exploit the analogy with a further phase diagram and ask questions about the nature of *transitions* between the different morphologies.

2. Formulation of the problem

We are interested in a non-equilibrium situation — growth of a stable phase from a metastable one. To be specific, we consider the two-dimensional growth of a pure substance from its undercooled melt, where the growth is controlled by the diffusion of the latent heat of freezing. It obeys the diffusion equation and appropriate boundary conditions at the moving (not known in advance) interface

$$\frac{\partial U}{\partial t} = D\nabla^2 U \tag{1}$$

$$v_n = D\vec{n}\cdot(\nabla U_S|_{int} - \nabla U_L|_{int}) \tag{2}$$

$$U|_{int} = \Delta - d(\Theta)K \tag{3}$$

The indices 'L' and 'S' refer to the liquid and solid, respectively. The specific heat, c_p, and the thermal diffusion constant D are considered to be the same in both phases, L is the latent heat; $U = (T - T_\infty)c_p/L$ is the appropriately rescaled temperature field measured from the imposed temperature T_∞ of the undercooled melt far away from the interface; in terms of these parameters,

$$\Delta = (T_M - T_\infty)\, c_p/L \tag{4}$$

is the dimensionless undercooling of the melt and T_M is the melting temperature.

The physics underlying Eqs. (1)–(3) is quite simple. A solidifying front releases latent heat which diffuses away as expressed by (1); requiring heat conservation at the interface gives (2) ($\vec{n}$ is the normal to the interface). Eq. (3) is the local equilibrium condition at the interface which takes into account the Gibbs–Thomson correction; K is the two-dimensional curvature and $d(\Theta)$ is the so-called anisotropic capillary length with an assumed fourfold symmetry,

$$d(\Theta) = d_0(1 - \epsilon\cos 4\Theta) \tag{5}$$

Here $d_0 = \gamma T_M c_p/L^2$ is a capillary length proportional to the isotropic part of the surface energy γ; Θ is the angle between the normal $\vec{n}$ to the interface and some fixed crystallographic direction, at which $d(\Theta)$ is minimal; ϵ is the strength of the anisotropy.

In Eq. (3) we neglect the kinetic effects, that is the dependence of the interface temperature on the growth velocity v_n which holds at the sufficiently small undercoolings and velocities.

Our main interest here is concerned with patterns which can grow at constant speed even at low undercoolings $\Delta < 1$, because if they exist they will dominate the systems behavior. A two-phase structure then must exist behind the growth front filling the space uniformly on sufficiently large scales. The fraction η of solid inside this two-phase region should be equal to Δ due to global conservation,

$$\eta = \Delta \tag{6}$$

One may define an envelope over the front of this complex two-phase structure, calling this suitably averaged envelope the *average front* in contrast to the local interface separating the solid from the

liquid. This average front can be considered as the real growth front in the sense that a two-phase mixture, solid plus liquid, grows into a one-phase region originally consisting of liquid only. These two-phase structures are developed from initially smooth interfaces by the well-known Mullins–Sekerka instability [15].

Eqs. (1)–(5) contain two-dimensional parameters, d_0 and D, and two dimensionless parameters, Δ and ϵ. It means that any characteristic length scale, ℓ, and growth velocity, v, of the possible structures can be presented in the form

$$\ell = d_0 f(\Delta, \epsilon), v = \frac{D}{d_0}\varphi(\Delta, \epsilon) \tag{7}$$

Our aim is to predict, for given undercooling Δ and anisotropy ϵ, the type of the two-phase structure, and its characteristic length scales and velocity, that is to calculate the functions f and φ in the relation (7). As it turns out these functions have scaling forms for small Δ and ϵ, thus showing power law dependencies on Δ and ϵ.

We construct the kinetic phase diagram in the plane (Δ, ϵ) (Fig. 2), which represents the regions of existence of different structures and the lines of transitions between the structures [1,2]. We discriminate between *compact* structures (C) and *fractal* structures (F). A complementary classification deals with the existence of orientational order. A structure with pronounced orientational order will be called *dendritic* (D), and without apparent orientational order it will be called *seaweed* (S).

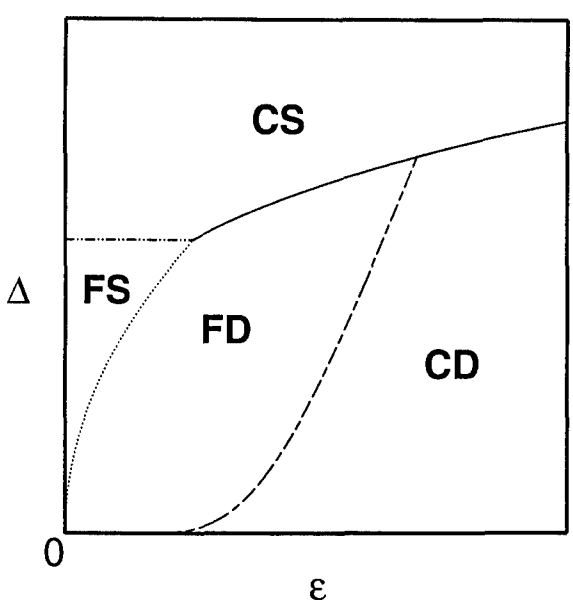

Fig. 2. Kinetic phase diagram.

It turns out that noise which always exists in the system (for example the thermodynamic noise) appears to play a crucial role in the formation of fractal structures but is not so important for compact patterns.

3. Compact dendrites (CD)

Dendrites can grow at arbitrary small undercooling Δ, but usually a non-zero value of the anisotropy ϵ is required. The growth pattern evolving from a nucleus acquires a star-shaped envelope surrounding a well-defined backbone. The distances between the corners of the envelope increase with time. For small undercooling we can use the scaling relation for the motion of the corners as for free dendrites [16–19] with tip radius ρ_t and velocity v. These two relations come from the Ivantsov formula [20]

$$P \equiv \frac{v\rho_t}{2D} \sim \Delta^2 \tag{8}$$

and from the selection condition for the stability parameter σ,

$$\frac{1}{\sqrt{\sigma}} \equiv \frac{\rho_t}{\sqrt{d_0 D/v}} \sim \epsilon^{-7/8} \tag{9}$$

It is quite remarkable that Eq. (8) was obtained in 1947 but it took about 40 years to derive the very non-trivial relation (9). One can find the details in [16–19]. From Eqs. (8) and (9) follow the dependencies of ρ_t and v on the parameters Δ and ϵ:

$$\rho_t \sim d_0 \epsilon^{-7/4}\Delta^{-2}, v \sim \frac{D}{d_0}\epsilon^{7/4}\Delta^4 \tag{10}$$

Eq. (10) really describes a needle-crystal which, without noise, has no sidebranches. The corresponding star structure then cannot fill the space with constant density and the amount of material solidified in parabolic form increases with time only according to $t^{3/2}$ rather than t^2 for a truly compact object in two dimensions.

A small amount of noise, however, cures this problem. The tip of the dendrite is still stable against small noise but has a 'convective' instability which produces sidebranches. Those branches continue to grow until they become independent primary branches a distance $\ell = D/v$ away from the corners of the star. The global shape then consists of an envelope of diamond type over the dendrite tips which appear a distance D/v apart from each other. The velocity scales like Eq. (10). The relative space filling by primary dendrites and sidebranches of course must be equal to Δ. The two basic length scales in this pattern accordingly are the diffusion length D/v and the tip radius ρ_t of a typical dendrite.

For small undercooling Δ those two length scales are well separated, $\rho_t \ll D/v$. While the dendritic structure becomes compact only at length scales larger than D/v, it shows fractal behavior at the intermediate length scale ℓ, $\rho_t < \ell < D/v$, with fractal dimension $D_f = 1.5$ [24]. In this fractal object the sidebranches interact due to the competition in the common diffusion field. Some of the sidebranches die and some continue to grow in the direction prescribed by the anisotropy. This competition leads to coarsening of the structure in such a way that the distance between the surviving sidebranches is adjusted to be of the same order of magnitude as the length of the sidebranches and is proportional to the distance from the dendritic tip. At the same time, the thickness of the surviving sidebranches is proportional to the square root of the product of ρ_t and the distance from the tip. On length scales larger than D/v the dendritic structure appears to be compact with mean density $\eta = \Delta$.

4. Compact seaweed (CS)

CD structures formally exist at arbitrary small anisotropy ϵ but their velocity goes to zero as $\epsilon \to 0$. It was recently discovered that there is another structure, compact seaweed (CS), which is favorable for smaller ϵ and larger Δ. The velocity of the structure remains finite at $\epsilon = 0$.

The compact-*seaweed* morphology [1,2] was originally introduced on the basis of experimental observations under the name *dense branching* morphology [25]. At that time, however, its introduction as a morphological 'phase' distinct from the well-known dendritic morphologies was rather speculative. Computer simulations also were inconclusive at that time.

The first indication for the existence of such a distinct phase came (to our knowledge) from arguments [1,2] based on a theoretical study of crystal growth in a channel [26]. This analysis of channel growth gave, among other things, the following results. A finger type pattern symmetrically in the center of the channel could grow at a constant growth rate for dimensionless supercoolings $\Delta > 0.5$. The finger looks similar to the Saffmann–Taylor finger of viscous flow, but belongs to a different branch of the mathematical solution. The growth rate of the crystal increases with increasing driving force Δ, as expected. A specifically remarkable result of this theory [26] is that the driving force sets a length scale and thereby also a velocity: For a given driving force $0.5 < \Delta < 1$ there exists a characteristic channel width below which such a steadily growing finger is no longer possible.

However, it has been discovered recently that the spectrum of solutions for growth in a channel is much richer than had previously been assumed. Parity-broken solutions were found [27] and studied numerically in detail [28–30]. A similar solution exists also in an infinite space which was called 'doublon' for obvious reasons [28,29]. It consists of two fingers with a liquid channel along the axis of the symmetry between them. It has a parabolic envelope with radius ρ_t and a liquid channel of thickness h. The Peclet number, $P = v\rho_t/2D$ depends on Δ according to the Ivantsov relation (8). The analytical solution of the selection problem for doublons [31] shows that this solution for isotropic systems ($\epsilon = 0$) exists even at arbitrary small undercooling Δ and obeys the following selection conditions:

$$h \sim \rho_t, \frac{1}{\sqrt{\sigma}} \equiv \frac{\rho_t}{\sqrt{d_0 D/v}} \sim P^{-5/4} \tag{11}$$

Eqs. (8) and (11) give

$$\rho_t \sim h \sim d_0 \Delta^{-7}, \quad v \sim \frac{D}{d_0} \Delta^9 \tag{12}$$

If one includes finite anisotropy ϵ, doublon solutions exist only above the solid line on Fig. 2, for which

$$\Delta \sim \epsilon^{1/4} \tag{13}$$

For ϵ smaller than that given by (13) the doublons obey the same scaling law as given by Eq. (12) [31].

It should be noted that doublons in the range of their existence (13), grow faster than dendrites for the same parameters Δ and ϵ. This statement is confirmed by numerical calculations [28,29].

The numerical calculations also show that the double-fingering structure is stable against competition between the two fingers which belong to the doublon. It means that the axis of symmetry and the direction of growth are stable. Of course these directions are arbitrary in isotropic systems. It is not completely clear at the moment if the stability of the free doublon pair follows precisely the scaling law Eq. (13). In any case this line represents a lower bound on Δ for a given ϵ.

We assume that the doublons seem to represent a key point in the growth of compact-seaweed morphology (Fig. 3). The formation of a full CS-structure evolving from a growing nucleus is possible only due to noise, which triggers sidebranches, as in the CD-structure. The resulting two-phase structure has an almost isotropic circular envelope which moves with approximately the same velocity [Eq. (12)] as a free doublon. The structure is fractal with $D_f = 1.5$ in the intermediate length scale between ρ_t and D/v, and it becomes compact with mean density $\eta = \Delta$ for the length scale larger than D/v. The region above the solid line, $\Delta \sim \epsilon^{1/4}$ (Fig. 2), corresponds to CS-structure where doublons exist and grow faster than dendrites. This line represents the discontinuous transitions between CD and CS-structures with a jump of velocities.

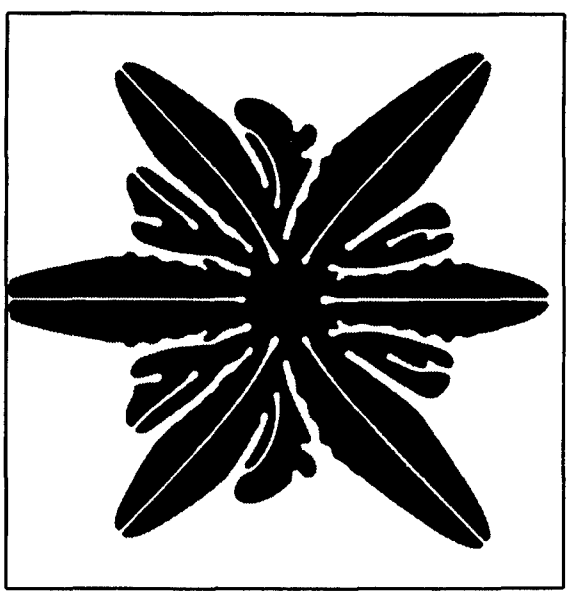

Fig. 3. Seaweed structure.

5. Surface dewetting as a diffusional growth process

As an application of this theory the effective equations of motion for a drying thin film wetting a substrate are derived. These equations are equivalent to the one-sided model of diffusional growth with an effective diffusion coefficient which depends on the viscosity and on the thermodynamic properties of the thin film.

According to the description given in [33], and also by Sharma [34,35] and de Gennes [36], there is a possibility for the almost dry part of the solid substrate to be in equilibrium with the wet part which is in fact a thin (but macroscopic) film of a liquid. Both parts (dry and wet) on the solid substrate are separated by an interface, which can be described by a height variable $h(x)$ with x being the coordinate across the interface from the dry to the wet part. Towards the dry part, the height variable goes to a very small value h_-, towards the wet part the film thickness goes to an equilibrium value $h_\infty(p)$ for given pressure p in coexistence with the vapor phase. At a specific pressure p_0 the liquid film can be also in equilibrium with the (almost) dry surface, the corresponding thickness of this wet film then is defined as $h_0 = h_\infty(p_0)$. For lower vapor pressure, the equilibrium film thickness $h_\infty(p)$ would decrease to a value smaller than h_0, but it would be metastable only and the the stable dry area would expand at the cost of the wet area. This is the dewetting phenomenon under consideration. Patterns similar to Fig. 3 have been recently observed experimentally [37].

We assume a surface-tension γ exists between the

liquid and the vapor. The free energy of the film then can be written as

$$G = \int \{g(h(x, y)) + \frac{\gamma}{2} |\nabla h|^2\} \, dx \, dy \tag{14}$$

In equilibrium a double-tangent construction to $g(h)$ gives two solutions of h_- for the dry part and of $h_0(p)$ for the wet part of the surface. This leads to the evolution equation [34,35,37] for the film variable $h(x,y;t)$:

$$\frac{\partial h}{\partial t} = \nabla \cdot \frac{h^3}{3\eta} \nabla \left[\frac{dg(h)}{dh} - \gamma \nabla^2 h \right] - \alpha \left[\frac{dg(h)}{dh} - \gamma \nabla^2 h - \mu(p) \right] \tag{15}$$

Note that a relaxational term proportional to α has been added. This term alone guarantees that a homogeneous liquid film will relax to its equilibrium value by evaporation or condensation. $\mu(p)$ is the chemical potential of the vapor. For $h = h_\infty(p)$ this term vanishes.

The first part of Eq. (15), proportional to the inverse viscosity η^{-1} of the liquid film, describes a creeping motion of a thin film flow on the surface. In the (almost) dry area the contributions of both terms to the total flow and evaporation of material can be basically neglected, because of the small value of h_-, typically less than one monolayer of adsorbed fluid. Inside the wet area we can to the lowest order linearize $h = h_\infty [1 + u(x, y)]$, where u is now a small deviation from the asymptotic equilibrium value for $h_\infty(p)$ in the liquid. Since $\nabla h_\infty(p) \equiv 0$ the only surviving terms are linear in u and its spatial derivatives ∇u and Δu. Therefore, inside the wet area, the evolution equation for the variable part u of the height variable h becomes

$$\frac{\partial u}{\partial t} = D_{\text{eff}} \Delta u - \lambda_{\text{eff}} u \tag{16}$$

We have dropped here the terms $\sim \gamma \Delta^2 u$ since the effective diffusion constant $D_{\text{eff}} = (h_0^3/3\eta)\{d^2g/dh^2\} + \alpha\gamma$ is positive and dominates the long-wavelength behaviour over the fourth-order term. The relaxation coefficient is $\lambda_{\text{eff}} = \alpha\{d^2g/dh^2\}$. Derivatives are taken around the equilibrium value $h = h_0$. Note that (16) now is precisely the equation of motion studied in [41], generalizing our basic model (Eq. (1)).

Of course, this approximation holds only inside the wet region, not directly at the dry–wet interface. This interface region gives rise to a profile $h(x)$ similar to a tanh function. The development of the tanh profile from the dry to the wet part occurs over a distance that is short compared to the typical patterns being observed in the dewetting process. We can therefore replace this profile by a sharp interface between the dry and the wet part, but must add the corresponding boundary conditions to the equation of motion (16) for the wet side. Obviously, the boundary conditions consist of a conservation law Eq. (2) which guarantees that a displacement of the dry–wet interface must locally conserve the fluid. Under dewetting conditions this leads to a swelling of fluid $u > 0$ at the interface. The second condition clearly comes from the surface tension γ which tends to keep the dry–wet interface straight. This is then just the usual Gibbs–Thomson condition for an interface, as described in Eqs. (3) and (4) above, with the capillary length being approximately $d_0 \approx \gamma/(\{d^2g(h)/dh^2\}\ell)$ where ℓ is the thickness of the dry–wet interface, and the dimensionless driving force is $\Delta = (h_0 - h_\infty)/h_0$. In summary, we have for this viscous fluid-flow problem of surface dewetting exactly the same equations as for the diffusional growth of an isotropic solid.

6. Fractal structures

For the compact structures described above noise is important only as the trigger of sidebranches. It has been assumed that the tips (of dendrites or doublons) remain undestroyed. However, the strength of noise may be large enough not only to trigger the sidebranches but also to destroy the tips. In order to estimate the parameters for which it happens let us look at the theory of sidebranch formation more carefully. According to the result of Langer [32] the root mean square amplitude, $\langle \zeta^2 \rangle^{1/2}$ of the sidebranches on the underlying parabolic interface generated by thermal fluctuations depends on the distance from the tip z according to

$$\frac{\langle \zeta^2 \rangle^{1/2}}{\rho_t} \sim \Gamma \exp\left[\frac{2^{7/4}}{3\sqrt{3\sigma}} \left(\frac{z}{\rho_t} \right)^{1/4} \right] \tag{17}$$

Here the stability parameter σ is given by Eqs. (9) and (11) for dendrites and doublons, respectively; Γ is the relative noise strength ($\Gamma \ll 1$)

$$\Gamma=(T/T_0)\left(\frac{2Dd_0^3}{v\rho_t^4}\right)^{1/2}, T_0=\left(\frac{L^2d_0^3}{k_B c_p}\right)^{1/2} \tag{18}$$

where k_B is the Boltzmann constant. The tip becomes destroyed if the amplitude of the sidebranches is of the order of ρ_t at the distance $z\sim\rho_t$ down the shaft. Thus we obtain from Eq. (14) the following condition

$$\frac{1}{\sqrt{\sigma^*}}\sim|\ln\Gamma| \tag{19}$$

The tips of the structures will be destroyed if the stability parameter σ becomes smaller than the critical value σ^* given by Eq. (16). Using the value $\sigma\sim\epsilon^{7/4}$ [Eq. (9)], one obtains from Eq. (16) a line of smooth transition from CD to FD-structures in Fig. 2:

$$\epsilon^*\sim|\ln\Gamma|^{-8/7} \tag{20}$$

The analogous line which separates CS and FS-structures in Fig. 2 can be obtained using Eqs. (8), (11) and (16):

$$\Delta^*\sim|\ln\Gamma|^{-2/5} \tag{21}$$

Eq. (16) has the following physical meaning. Let us rewrite this relation, using the definition of $\sigma=d_0D/(v\rho_t^2)$ [Eq. (9)], which gives the following condition for a stable tip radius:

$$\rho_t\le\rho_{MS}|\ln\Gamma| \tag{22}$$

where $\rho_{MS}\sim\sqrt{d_0D/v}$ is the Mullins–Sekerka length describing the instability of a planar interface. One can think of the right-hand side of (19) as the characteristic length scale, a_Γ, of the instability due to noise

$$a_\Gamma=\rho_{MS}|\ln\Gamma|\sim\sqrt{d_0D/v}\,|\ln\Gamma| \tag{23}$$

The tip is stable if $\rho_t<a_\Gamma$ and it becomes destroyed if $\rho_t>a_\Gamma$. The same small-size cutoff a_Γ depending on noise Γ was introduced in our previous paper [1,2] based on the consideration of the self-similar development of perturbations induced by the Mullins–Sekerka instability. At that time, however, the existence of doublons was not known.

A new approach, therefore, is required for the description of the fractal patterns with the destroyed tips. Such destroyed fractal structures have been already investigated in the framework of Saffmann–Taylor viscous fingering and diffusion-limited aggregation [21–23]. The important result of these investigations is that there exists an effective envelope obtained by averaging over the structures, which has precisely the same shape as an ideal stable solution — the shape of the Saffmann–Taylor finger in isotropic systems and parabolic shape in anisotropic systems. The density inside this effective envelope is $\tilde\eta<1$. The envelope has a characteristic tip radius $\tilde\rho_t$. Because the underlying structure is fractal with fractal dimension $D_f\approx1.71$ in the intermediate length scale between small-length cutoff a_Γ and $\tilde\rho_t$, the density $\tilde\eta$ inside the envelope can be obtained from the definition of the fractal dimension (apart from a constant prefactor)

$$\tilde\rho_t^{D_f}\sim\int_{a_\Gamma}^{\tilde\rho_t}\mathrm{d}r\,r\tilde\eta(r)$$

which gives more explicitly

$$\tilde\eta(\tilde\rho_t)\sim\left(\frac{a_\Gamma}{\tilde\rho_t}\right)^{2-D_f} \tag{24}$$

Following these results, we will now try to define an averaged or coarse-grained structure over such a noisy fractal pattern and to formulate an equation of motion for this coarse-grained structure using scaling arguments. More explicitly we try to estimate the characteristic length scale of the structure and its growth velocity by considering the steady-state motion of an effective parabolic envelope which replaces the destroyed dendrite or doublon. The density of the solid phase inside the envelope with tip radius $\tilde\rho_t$ is given by Eq. (21), where the small size cutoff a_Γ is defined by Eq. (20)

$$\tilde\eta(\tilde\rho_t)\sim\left(\frac{\sqrt{d_0D/v}|\ln\Gamma|}{\tilde\rho_t}\right)^{2-D_f} \tag{25}$$

The temperature inside the envelope is assumed to be close to the melting temperature. Because the density $\tilde\eta$ inside the envelope is smaller than 1, we have to

replace the latent heat L by $\tilde{\eta}L$. It changes Δ in Eq. (4) to $(\Delta/\tilde{\eta})$ and modifies the Ivantsov relation to

$$P \equiv \frac{v\tilde{\rho}_t}{2D} \sim \left(\frac{\Delta}{\tilde{\eta}}\right)^2 \tag{26}$$

The crucial point of the analysis is a modification of the selection conditions (9) and (11). The experimental and numerical results [21–23] (the existence of a selected envelope) support the idea that those selection conditions do exist. Unfortunately, we do not know any results which allow us to write down these modifications explicitly. But, using scaling arguments, we can write the selection conditions in the following scaling form with scaling exponent β which for the moment is undetermined but will be specified later. For dendrites we can write

$$\frac{1}{\sqrt{\sigma}} \equiv \frac{\tilde{\rho}_t}{\sqrt{d_0 D/v}} \sim \epsilon^{-7/8}\, \tilde{\eta}^{-\beta} \tag{27}$$

and for doublons

$$\frac{1}{\sqrt{\sigma}} \equiv \frac{\tilde{\rho}_t}{\sqrt{d_0 D/v}} \sim P^{-5/4}\, \tilde{\eta}^{-\beta} \tag{28}$$

These relations (24) and (25) transform into Eqs. (9) and (11), respectively, for $\tilde{\eta} \sim 1$.

The selection relations (24) and (25) may be interpreted as the conditions of selection due to an effective surface tension. We have chosen the same β in both Eqs. (24) and (25) because in some sense the factor $\tilde{\eta}^{-\beta}$ can be seen as a renormalization factor for the capillary length $d_0 \to d_0/\tilde{\eta}^{2\beta}$. To make an estimate of possible values of β it is natural to assume that a coarse-grained surface energy should decrease with decreasing $\tilde{\eta}$, giving $\beta < 1/2$ as a reasonable restriction. We have shown [1,2] that the scaling exponent β can be expressed in terms of bulk D_f and surface D_s fractal dimensions:

$$\beta = \frac{1}{2}\left(1 - \frac{D_s - 1}{2 - D_f}\right) \tag{29}$$

All the characteristics of fractal structures depend on the noise strength Γ. We can estimate Γ in the fractal region using Eq. (15) and replacing ρ_t by the noise-induced length scale a_Γ from Eq. (20). It gives

$$\Gamma\,|\ln\Gamma|^2 \sim \left(\frac{T}{T_0}\right)\left(\frac{vd_0}{D}\right)^{1/2} \tag{30}$$

The noise strength $\Gamma \ll 1$ because the capillary length d_0 is much smaller the diffusion length D/v.

7. Conclusion

We have discussed the structure formation in diffusion-controlled growth. The given description refers to solidification of a pure undercooled melt but it also can be applied to growth of a pure solid from solution or isothermal solidification of a binary melt. More generally one may speak of systems with a conserved quantity growing by diffusion. The main control parameters of the process are dimensional undercooling Δ and the strength of the surface tension anisotropy ϵ. It turns out that the noise is also very important for the structure formation and we characterize it by the dimensionless quantity Γ.

The resulting morphology diagram (Fig. 2) with axes Δ vs. ϵ classifies different kinds of structures and transitions between them.

The dendritic structure has pronounced orientational order and it is favorable for small Δ and relatively large ϵ. The seaweed structure does not require anisotropy and is favored for larger Δ and smaller ϵ. The transition between these two structures takes place around the solid line on Fig. 2 [Eq. (13)] which is continued by the dotted line into the fractal region. This transition is discontinuous with a jump of velocities since the doublons move faster than the dendrites as soon as they exist. The main element of the dendritic structure is a dendrite with a parabolic tip, and the main element of the seaweed structure is a doublon (Fig. 3). For compact dendritic and compact seaweed structures the tips of dendrites and doublons are stable against the noise which is relatively small in these regions. The noise triggers sidebranches which fill the space and make the structures compact so that the mean density of the solid phase is $\eta = \Delta$ on the length scale larger than D/v. In the intermediate region of lengths between the tip radius ρ_t and diffusion length D/v the structure can be described as a fractal but with a trivial fractal dimension $D_f = 3/2$ which comes from the parabolic shape of the dendrite.

The region of fractal dendritic and fractal seaweed structures near the origin of the morphology diagram is characterized by noise being sufficiently large to

destroy even the tips of dendrites and doublons. It means that the noise-induced length scale a_l [Eq. (20)] is smaller than $\tilde{\rho}_t$. In the range between a_l and $\tilde{\rho}_t$ the structures are fractal with a non-trivial fractal dimension D_f ($D_f \approx 1.71$). This is the reason why we called these structures 'fractal'. Furthermore, these patterns are also fractal in the range between $\tilde{\rho}_t$ and D/v but again with the trivial fractal dimension $D_f = 3/2$. Finally they become compact on length scales larger than the diffusion length D/v just as compact dendritic and compact seaweed structures. Note that if one performed a measurement of the fractal dimension on length scales around the cross-over length $\tilde{\rho}_t$ one would observe an interpolation between our two different values of D_f, the precise result depending on the interval chosen for the measurement. Since both the dendritic and the seaweed patterns maintain their basic identities inside the noisy region the transitions from the compact to the fractal regions represent rather smooth changes in length scales.

We have described the structures and growth velocities of the destroyed fractal dendrites and doublons by introducing renormalized quantities for capillary length and density. We have quantitatively introduced an effective parabolic envelope following the results of [22–24]. The most non-trivial part of our analysis is a modification of the selection conditions [Eqs. (24) and (25)]. At this point we have used scaling arguments which leave us only with one undetermined scaling exponent β. This exponent subsequently is determined by the fractal dimensions D_s for the surface and D_f for the bulk of the growing pattern. The closed set of equations for the growth rate and the tip radius are Eqs. (22)–(24) for fractal dendritic growth, and Eqs. (22), (23) and (25) for fractal doublon growth. The two-dimensional theory together with a small modification [41] in addition explains the patterns observed on a solid surface which was covered by a thin wetting layer of fluid. When a dry spot nucleates in this layer dewetting occurs through the propagation of the essentially one-dimensional separation line between the wet and the dry parts of the surface. Doublon structures then can be clearly observed.

The scaling arguments given here for two-dimensional growth patterns formally can be extended in a straightforward fashion to three dimensions. For dendritic structures this seems to be perfectly permissible since the basic growth laws are rather similar in two and three dimensions [38,39]:

$$\rho_t \sim d_0\, \epsilon^{-7/4}\, |\ln \Delta|/\Delta,\ v \sim \frac{D}{d_0}\, \epsilon^{7/4}\, (\Delta/\ln \Delta)^2 \qquad (31)$$

(compare to Eq. (10) for 2-D). There is, however, the crucial difference between the 3-D and the 2-D case. In the later, small anisotropy implies that the shape of the selected needle crystal is close to the Ivantsov parabola everywhere; in the former, strong deviations from the Ivantsov paraboloid appear for any anisotropy. This shape, in units of the tip radius of curvature, depends mostly on the crystalline symmetry and it is almost independent of the material and growth parameters. The shape of the 3-D dendrite, which has been described analytically [39], together with sidebranching activity [24] is presented in Fig. 4. For the seaweed patterns much less is known since our preliminary results are mostly numerical ones [40] (Fig. 5). The crucial point here is that this self-organized triplet structure is not imposed by the symmetry of the calculation box and it consists of three cooperating symmetry-broken fingertips. A hexagonal or triplet structure should be expected to occur under free growth conditions from the basic symmetry considerations, since these growth problems do not have reflection symmetry about some

Fig. 4. 3-D dendrite.

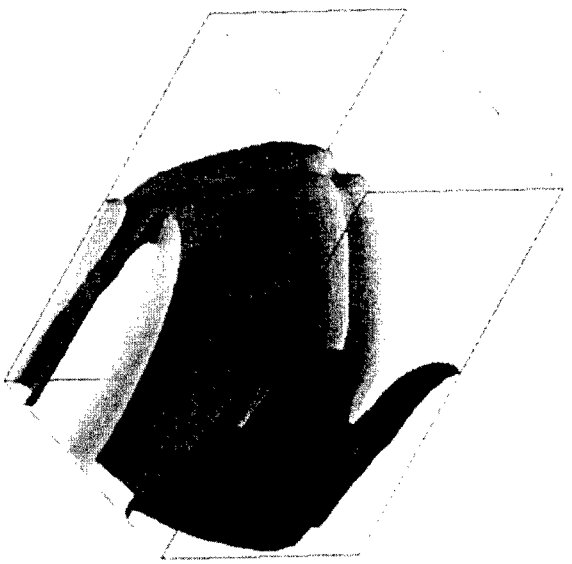

Fig. 5. 3-D triplon.

average interface position. The resulting multiplets consisting of symmetry-broken cooperating fingers of the growing phase finally seem to be the basic building blocks for the compact seaweed morphology, in particular the triplet structure appears to be characteristic for free growth. We expect these triplons even to appear in systems with convection driven by surface tension, provided the growth rate is faster than the convection rate defined as the ratio of surface tension divided by viscosity. At present, however, there is still a need for detailed experiments in this region of low crystalline anisotropy but rather high driving force.

References

[1] E. Brener, H. Müller-Krumbhaar, D. Temkin, Europhys. Lett. 17 (1992) 535.
[2] E. Brener, H. Müller-Krumbhaar, D. Temkin, Phys. Rev. E 54 (1996) 2714.
[3] T. Kobayashi, T. Kuroda, in: I. Sunagawa (Ed.), Morphology of Crystals, Vol. Part B, Terra Scientific Publishing, Tokyo, 1987, p. 645.
[4] J. Kepler, The Six-Cornered Snowflake, Clarendon Press, Oxford, 1966 (translated by C. Hardie); originally published as Seu de Nive Sexangula, Godfrey, Tampach, Frankfurt am Main, 1611.
[5] M.E. Glicksman, R.J. Shaefer, J.D. Ayers, Metall. Trans. A 7 (1976) 1747.
[6] S.C. Huang, M.E. Glicksman, Acta Metall. 29 (1981) 701.
[7] S.C. Huang, M.E. Glicksman, Acta Metall. 29 (1981) 717.
[8] M.E. Glicksman, Mater. Sci. Eng. 65 (1984) 45.
[9] N. Goldenfeld, J. Cryst. Growth 84 (1987) 601.
[10] E. Ben-Jacob, G. Deutscher, P. Garik, N.D. Goldenfeld, Y. Lereah, Phys. Rev. Lett. 57 (1986) 1903.
[11] S.N. Rauseo, P.D. Barnes, J.V. Maher, Phys. Rev. A 35 (1987) 1245.
[12] Y. Couder, in: H.E. Stanley, N. Ostrowsky (Eds.), Random Fluctuations and Pattern Growth: Experiments and Models, Kluwer Academic Publishers, Dordrecht, 1988, p. 75.
[13] P. Ossadnik, Phys. Rev. A45 (1992) 1058.
[14] E. Ben-Jacob, P. Garik, Physica D 38 (1989) 16.
[15] W. Mullins, R. Sekerka, J. Appl. Phys. 34 (1963) 323.
[16] J.S. Langer, in: J. Souletie, J. Vannimenus, R. Stora (Eds.), Chance and Matter, Elsevier, Amsterdam, 1987.
[17] D.A. Kessler, J. Koplik, H. Levine, Adv. Phys. 37 (1988) 255.
[18] E.A. Brener, V.I. Mel'nikov, Adv. Phys. 40 (1991) 53.
[19] Y. Pomeau, M. Ben Amar, in: C. Goldréche (Ed.), Solids Far from Equilibrium, Cambridge University Press, Cambridge, 1992.
[20] G.P. Ivantsov, Dokl. Acad. Nauk. SSSR 58 (1947) 567.
[21] A. Arneodo, Y. Couder, G. Grasseau, V. Hakim, M. Rabaud, Phys. Rev. Lett. 63 (1989) 984.
[22] Y. Couder, F. Argoul, A. Arneodo, J. Maurer, M. Rabaud, Phys. Rev. A 42 (1990) 3499.
[23] A. Arneodo, F. Argoul, Y. Couder, M. Rabaud, Phys. Rev. Lett. 66 (1991) 2332.
[24] E. Brener, D. Temkin, Phys. Rev. E 51 (1995) 351.
[25] E. Ben-Jacob, G. Deutscher, P. Garik, N. Goldenfeld, Y. Lereah, Phys. Rev. Lett. 57 (1986) 1903.
[26] E. Brener, M. Geilikman, D. Temkin, Sov. Phys. JETP 67 (1988) 1002.
[27] E. Brener, H. Müller-Krumbhaar, Y. Saito, D. Temkin, Phys. Rev. E 47 (1993) 1151.
[28] T. Ihle, H. Müller-Krumbhaar, Phys. Rev. Lett. 70 (1993) 3083.
[29] T. Ihle, H. Müller-Krumbhaar, Phys. Rev. E 49 (1994) 2972.
[30] R. Kupfermann, D. Kessler, E. Ben-Jacob, Physica A 213 (1995) 451.
[31] M. Ben Amar, E. Brener, Phys. Rev. Lett. 75 (1995) 561.
[32] J.S. Langer, Phys. Rev. A 36 (1987) 3350.
[33] L. Landau, E. Lifshitz, Statistical Physics, Akademie-Verlag, Berlin, 1970.
[34] A. Sharma, A.T. Jameel, JCIS 161 (1993) 190.
[35] A. Sharma, A.T. Jameel, JCIS 164 (1994) 416.
[36] P.G. de Gennes, Rev. Mod. Phys. 57 (1995) 827.
[37] N. Samid-Merzel, S.G. Lipson, D.S. Thannhauser, Physica A, in press.
[38] M. Ben Amar, E. Brener, Phys. Rev. Lett. 71 (1993) 589.
[39] E. Brener, Phys. Rev. Lett. 71 (1993) 3653.
[40] E. Brener, H. Müller-Krumbhaar, D. Temkin, T. Abel, Physica A 249 (1988) 73.
[41] T. Ihle, H. Müller-Krumbhaar, J. Phys. I France 6 (1996) 949.